STRAIN RATE DEPENDENT MECHANICAL BEHAVIOR OF NANOSTRUCTURED MG-3%AL ALLOYS

Ashis Mallick*, Surja Deka, Vivek Kr. Sharma, Ashutosh Kumar

Department of Mechanical Engineering, Indian Institute of Technology (ISM) Dhanbad, India

Abstract

This work focused on the strain rate-dependent mechanical behavior of Mg-3%Al alloy fabricated via powder metallurgy. The effects of ball milling for different durations are also discussed in this study. Powder metallurgy approach integrating sintering at inert atmosphere followed by hot extrusion was used to fabricate Mg-3%Al alloys. Microstructural analysis and X-ray diffraction (XRD) studies demonstrated that the alloy of the solid solution of Mg and 3%Al were successfully fabricated using the powder metallurgy route. Both the milled powder and their extruded bulk samples revealed evidence of the formation of second-phase particles. Tensile tests were carried out at different strain rates, and the yield strength, tensile strength, and elongation to failure of samples made from milled and un-milled powders were measured and compared. The findings demonstrated that the strain rate and the grain sizes of the extruded samples have a significant impact on the strength and ductility of the bulk samples. The possible deformation mechanisms for each sample are discussed. It is hypothesized that the grain boundary movement mechanism and the geometrically necessary dislocations primarily governs the deformation process. The possible fracture mechanisms were predicted from the microstructural study of the fracture behaviors of the deformed samples. The micro-mechanical properties of each sample were analyzed using the loading-unloading curves of the micro-indentation test.

Keywords: *Mg alloy, powder metallurgy, strain rate, mechanical alloying, mechanical properties*

1. INTRODUCTION

Following World War II, officials from all participating countries recognized that materials were the limiting factor for advancements in space and military technologies. Since then, there has been a considerable demand for innovative and advanced engineering materials with improved modern technology in the different fields of engineering. In order to satisfy this growing need, innovations in the development of materials have forced researchers to think of materials that have light weights, high specific strengths, good wear and corrosion resistance, and are biocompatible and biodegradable.

In recent years, rapid research advancements on Mg-based light-weight and high-specific-strength materials have been seen [1-2]. Magnesium alloys and their composites have become increasingly appealing to the researchers for their wide range of technological applications, particularly in the automotive, aerospace, sports, electronics, and biomedical industries [3-5]. However, due to strong affinity towards oxygen, the dealing of Mg during the fabrication process of their alloys and composites is a real challenge for engineers and scientists. In addition, because of their hcp structure, Mg based materials suffer from poor plasticity, low strength, and poor resistance to corrosion. These constraints are often circumvented by the adding of appropriate alloying elements to produce an alloy. Further, grain refinement by reducing grain size to the nanoscale range is another smart strategy for enhancing the mechanical properties of Mg based materials [6]. In general, nanostructured Mg-alloys have better strength and simultaneously maintain significant ductility as compared to coarse-grained alloys [7]. Thus, a comprehensive experimental study for the proper design of Mg-based materials based on the applications is of the utmost necessity.

Open literature reveals that Mg and its alloys have many deformation processes because of their hexagonal-closed-packed crystalline structure and play different roles at the same time under different loading conditions [8]. The room-temperature deformation processes for Mg alloys include basal slip, prismatic slip, pyramidal slip, and extension twinning [9]. During slip-dominated deformation processes such as in-plane tension, these alloys exhibit to have high strain rate sensitivity. Zhang et al. [10]

demonstrated that strain rate has a profound effect on the tensile behavior of Mg–9Y–3Zn–1Mn alloy. Their study also revealed that the strain rate effect was more pronounced on the ductility of the alloy as compared to its strength.

In view of the aforementioned discussion, the objective of this research work is to investigate the rate dependent mechanical behavior of nanocrystalline Mg-3%Al alloys. The alloys were synthesized using powder metallurgy route, where the micron-sized primary powders of Mg and Al were mechanically alloyed (MA) using high energy ball milling over a prolonged period of time. The impacts of milling durations on the microstructural behavior and mechanical properties of synthesized materials were also examined in this paper. The summary of the present study is presented in the form of a flow diagram in Fig.1.

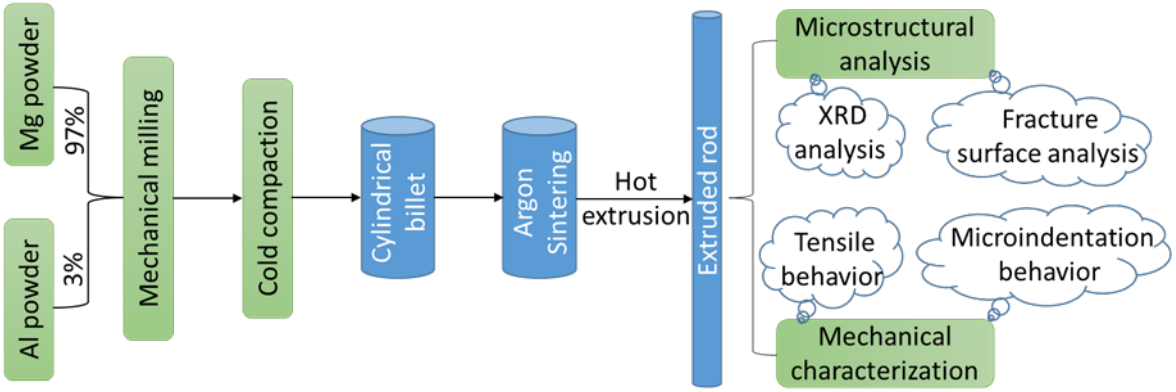

Fig. 1. Schematic representation of the present study

2. MATERIALS AND METHODS

2.1. Materials

In order to develop Mg-3%Al alloy, pure commercial magnesium (Mg) powder with a purity of 98.5% and pure commercial aluminum (Al) powder with a purity of 99.5% were used as elemental powders for blending. The blending of the powders ensured the homogeneity of the mixtures. The typical particle size of Mg (supplied by Merck, Germany) was 60-300 µm, and the particle size of Al powder (supplied by Alfa Aesar, USA) was 5-15 µm. Magnesium was chosen as a base material due to its low structural density and high specific strength, while Al was considered as an alloying element due to its ability to improve Mg strength and ductility.

2.2. Methods

2.2.1. Alloy development

Magnesium and aluminum powders were precisely weighed in a fully automatic electronic weighing machine (Model No.: AB30-S, Mettler Toledo, Switzerland) with a precision of up to 1.0 µg, and then dried in vacuum for two hours at 200 °C. The elemental powders, Mg and Al, were mixed in a 97:3 weight ratio of Mg to Al. For mechanically milling the mixture of the dried powders, stainless steel spherical balls having 15 mm diameter were utilized in a stainless steel vial with a weight ratio of around 20:1 ball-to-powder. Prior to milling, 2 wt.% stearic acid was added to the powder mixture in order to prevent the powders from agglomerating and excessively cold welding. In order to obtain three different batches of milled powders, the mechanical alloying was carried out for 10 hrs, 20 hrs, and 30 hrs in a RETSCH PM 400 mechanical alloying machine. In order to better mixing and prevent from an excessive heat generation during the milling, the machine was run at 250 rpm rotational speed in a sequence of 30 minutes in a clockwise direction, followed by a 30 minute break and 30 minutes of anticlockwise direction. The milled powders were loaded into a hollow cylindrical die, and a plunger was put on top of the powders in the die. To avoid oxidation, the powders (both milled and un-milled) were handled all

times in a glove box occupied with a highly refined (~99.9% purity) argon gas. The mechanically alloyed particles were consolidated by cold compaction using an isostatic load of 50 tons (97 bar pressure) to yield a cylindrical billet of 35 mm in diameter and 35 mm in height. The billets were then sintered at 450 °C for 2 hrs in an Argon furnace to fuse the compacted powders together tightly. The sintered billets were extruded at an extrusion temperature of 350 °C with a 25:1 extrusion ration to produce a 7 mm cylindrical rod. The un-milled bulk sample was likewise fabricated for subsequent comparison.

2.2.2. X-ray diffraction analysis

The constituent phases and texture variations of the mechanically alloyed powder and the extruded samples were examined by X-ray peak profile analysis. An automated Shimadzu LAB-X-6000 X-ray diffractometer (XRD) with Cu K_α radiation (λ= 1.5406 Å) was operated at 30 kV and 40 A with a scanning speed of 2°/min. The average grain sizes of milled powders and their extruded samples were estimated using the Hall-Williamson method.

2.2.3. Tensile tests

The tensile properties of Mg/3%Al alloys were studied at different strain rates. The extruded rods of 7 mm dia were machined in a CNC machine to produce round cross-sectioned dog-bone type tensile specimens with gauge diameter of 5 and 25 mm gauge length in compliance with ASTM E8M-96 standard for tensile testing. Tests were conducted at various strain rates on a fully computer controlled servo-hydraulic Instron-8874 universal testing machine (UTM) with a load cell of 25 kN and sensitivity of 5N. Tensile properties were estimated based on the average of three tests for each test condition.

2.2.4. Micro-indentation tests

The microindentation measurements of the alloys were carried out using a load-controlled, completely automated MTR3/50-50/NI instrument supplied by MICROTEST S.A., Spain. In order to examine the rate dependent micro-mechanical behavior of the alloy, the samples were loaded and unloaded at three different loading rates (5 N/min, 2.5 N/min, and 1 N/min) for each group of alloys. A Vickers indenter with an upright pyramid diamond tip and a 136° angle between opposite faces at the vertex was employed for indentation. The samples were metallographically polished before the indentation test to ensure their smooth surface. All indentation tests were carried out at a controlled ambient temperature of 24 °C. At least three indentations at different positions of each sample for each loading rates were carried out to obtain a reproducible result.

3. RESULTS AND DISCUSSION

The mechanical properties of the material are one of the most important determinants of its potential applications. In this study, the experimental results of mechanically alloyed bulk Mg-3% Al alloys was found to have several remarkable strain rate as well as loading rate dependent mechanical properties. The alloy fabricated from 10 hrs milled powder exhibits a dramatic increase in strength with fair ductility, whereas the sample obtained from longer milling durations exhibits a decrease in strength along with much improved ductility and a near-perfect elastoplastic behavior. Several possible interpretations for the observed phenomena can be offered in light of the observed microstructural and physical behavior.

X-ray diffraction line profiles as shown in Fig. 2 were used to examine the crystallographic structure of the mechanically alloyed powders and their extruded solid samples of Mg-3%Al alloys. All of the XRD spectrums show that α-Mg is the most dominant phase. In Fig.2a, the XRD spectrum of the un-milled powder detects the alloying element Al diffraction peak (1 1 1), whereas the Al peak is totally disappeared in the extruded samples consolidated from the un-milled powders (Fig.2b). This result suggests that a solid solution of Mg and 3% Al elemental powders formed during the mechanical alloying. The $Mg_{17}Al_{12}$ peak (3 3 2) was identified in the milled powder sample. The full width at half maximum (FWHM) of Mg peaks broadened with increasing milling durations. The broadening of the Mg peak at the same diffraction angle (2θ) with increasing milling time suggests the formation of microstrains and the reduction of grain size. The $Mg_{17}Al_{12}$ peak became less intense in the XRD line

profile of the extruded samples. Rather, new traces of $MgAl_2O_4$ oxide were found in the extruded milled samples, and their peaks were more intense in the samples with longer milling times. These findings demonstrated the formation of oxide particles during longer-duration of milling and powder consolidation processes. The solid-solid reactions of the MgO oxide layer on the surface of the Mg powder and the Al_2O_3 oxide layer on the surface of the Al particles may have been favoring the formation of $MgAl_2O_4$ during prolonged mechanical milling and consolidation processes. A weaker Mg (0 0 2) peak in the extruded samples suggest that the basal plane rotates favorably in the direction of [1 0 1] to coincide with the extrusion direction. On the other hand, the diffraction peaks (1 0 0) and (1 1 0) of Mg were intensified, indicating textured structure. The grain sizes of the milled powders and their extruded samples were estimated from FWHM using the Hall-Williamson method. The grain sizes for the 10 hrs, 20 hrs, and 30 hrs milled powders were estimated ~94 nm, ~ 40 nm, and ~30 nm, respectively, while ~178 nm, ~120 nm, and ~90 nm were predicted for the corresponding extruded samples. A similar observations were reported earlier in our published articles [7].The optically measured average grain size of the un-milled extruded sample was about 13 μm.

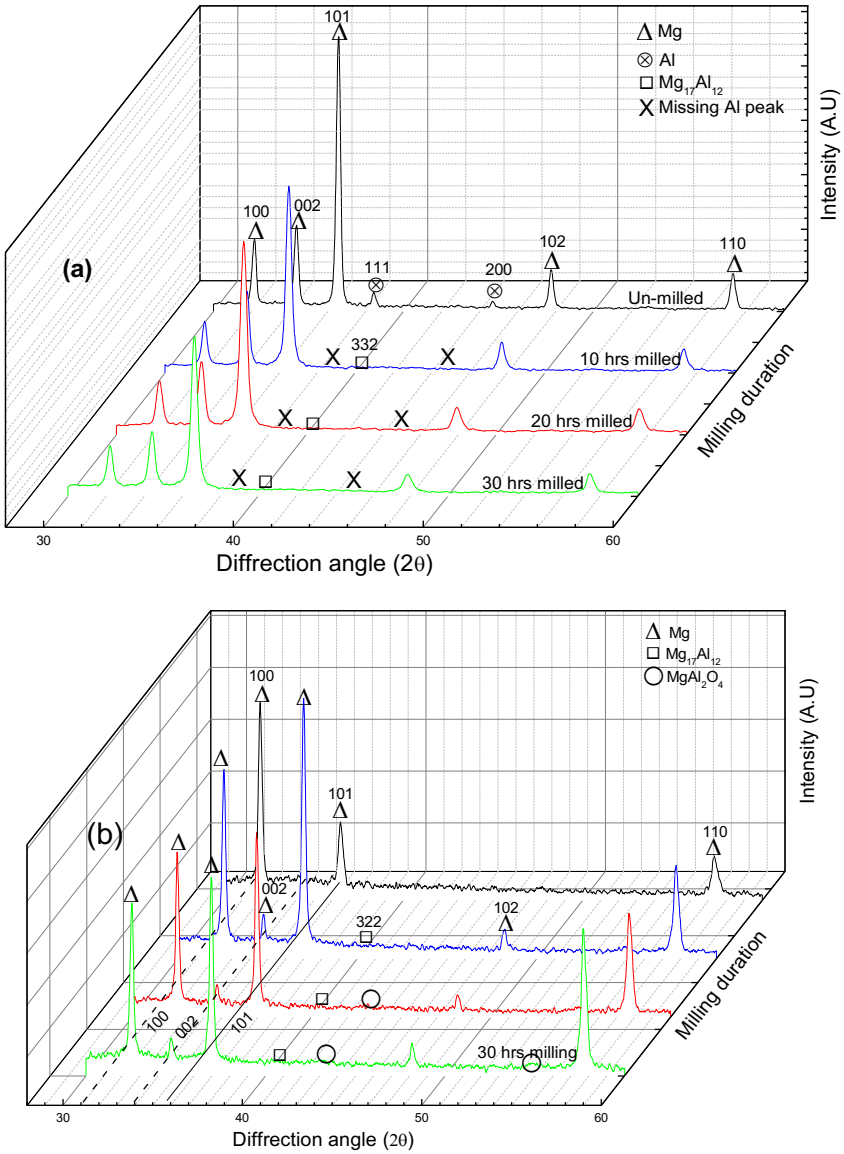

Fig. 2. X-Ray diffraction line profiles of the powder and extruded solid samples of (a) powder samples (b) bulk extruded samples.

Fig. 3 represents the true tensile stress-strain curves of the extruded samples obtained from different milling durations. The curves were plotted at room temperature at different strain rates ranging from 4×10^{-5} s^{-1} to 4×10^{-3} s^{-1}. The stress-strain curves up to fracture demonstrate that strain rate has a significant effect on tensile deformation behaviors for of all the cases. The yield strength and ultimate strength of all kind of samples increase with the increase of strain rates. The increase in strain rate induces an increase in dislocation density and, consequently, a rise in stress level. In contrast, with a few exceptions, the specimen elongation demonstrates opposing tendencies when strain rate increases in the range of strain rates considered here. Moreover, it can be observed that the milling duration had a substantial effect on the strength and failure strain of samples tested at various strain rates. The un-milled samples exhibit work hardening at all strain rates. Conversely, for all strain rates, the samples with 10 hrs milling show nearly perfect elastic-plastic behavior. For 20 hrs and 30 hrs milled samples, elastic followed by plastic behavior along with a brief softening phase can be seen at all strain rates. The strength of the 10 hrs milled sample is significantly higher than that of the un-milled sample and 20 hrs and 30 hrs milled samples. At strain rate strain rate 4×10^{-4} s^{-1}, 10 h milled sample has ~ 245 YS and ~433 MPa UTS, whereas the 0 h, 20 h and 30 h milled samples have ~164 MPa YS and ~305 MPa UTS, ~179 MPa YS and ~254 MPa UTS, and 165 MPa YS and ~230 MPa UTS, respectively. The substantial improvement in strength in the sample milled for 10 h is a result of grain refinement in accordance with the Hall-Pitch relationship. The large grain boundary network of the refined grain structure, which serves as an obstacle to the migration of any dislocations and twinning, may be the mechanism for the increase in strength. While further milling reduces strength, this might be due to the activation of grain boundary sliding and diffusion that reduces work hardening. All the milled samples exhibited large strain when compared to the un-milled sample, and the strain to failure value increases with the increase of milling time. The enhanced ductility in the milled samples is a result of grain boundary deformation mechanisms such as grain boundary diffusion, interfacial sliding, and grain boundary shear.

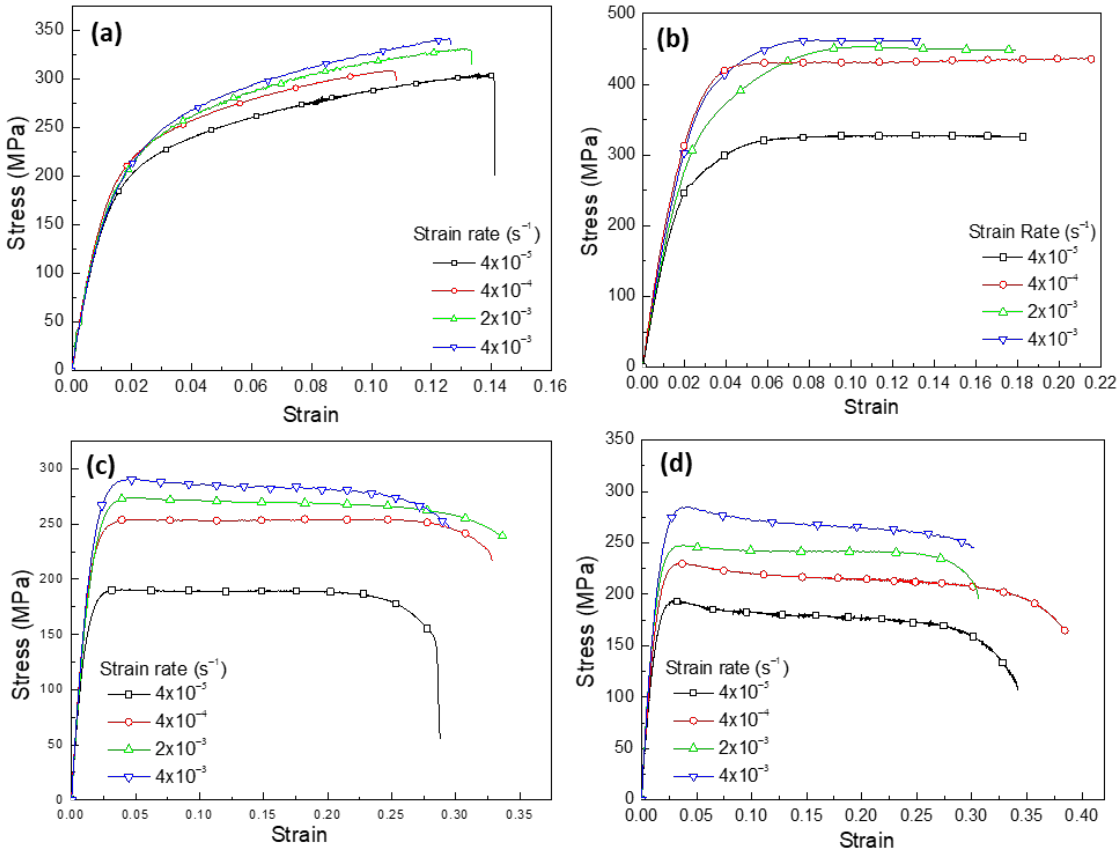

Fig. 3. True stress-strain tensile curves at different strain rates: (a) un-milled sample, (b) 10 hrs milled sample, (c) 20 hrs milled sample and (d) 30 hrs milled sample.

Table 1 lists the summary of yield strength (YS), ultimate tensile strength (UTS), and tensile elongation (%) for each category of the sample tested at various strain rates. It can be seen that the sample with 10 hrs milling exhibit higher yield strength and ultimate strength, as well as reasonable ductility for all the strain rates. The ability of fine grains to store dislocations at a higher rate resulted in increased ductility due to delayed necking [11].

Milling	**SR = 4×10^{-3} s^{-1}**			**SR = 4×10^{-4} s^{-1}**			**SR = 4×10^{-5} s^{-1}**		
Time (hrs.) ↓	YS (MPa)	*UTS* (MPa)	% ε_f	YS (MPa)	*UTS* (MPa)	% ε_f	YS (MPa)	*UTS* (MPa)	% ε_f
0	143.9	342.0	12.6	164.1	305	11.0	140.8	304.0	14.1
10	276.3	462.5	14.0	245.2	433.8	21.5	16.5	325.2	18.3
20	189.1	291.3	29.53	179.5	254.1	32.5	137.1	189.1	28.4
30	197.6	284.1	30.0	165.7	229.9	38.4	147.6	192.2	34.1

*YS → Yield strength, UTS → Ultimate tensile strength, and ε_f → percentage of failure strain.

Table 1. Room temperature tensile properties of Mg/3%Al alloy at different strain rates.

Figure 4 illustrates the fracture surfaces of un-milled and milled tensile specimens tested at room temperature with a strain rate of 4×10^{-4} s^{-1}. The fracture surface of the un-milled sample (Fig. 4a) is very rough and cleavage-type owing to the larger particle size. In contrast, the milled samples exhibited "grain-like" shearing pattern with a finer structure on the fracture surfaces (Fig. 4b-4d). Two distinct fracture modes are observed: (a) an intergranular mode is associated with the fracture surface of fine-grained milled samples, (b) whereas the transgranular cleavage mode is observed in coarse-grained un-milled samples.

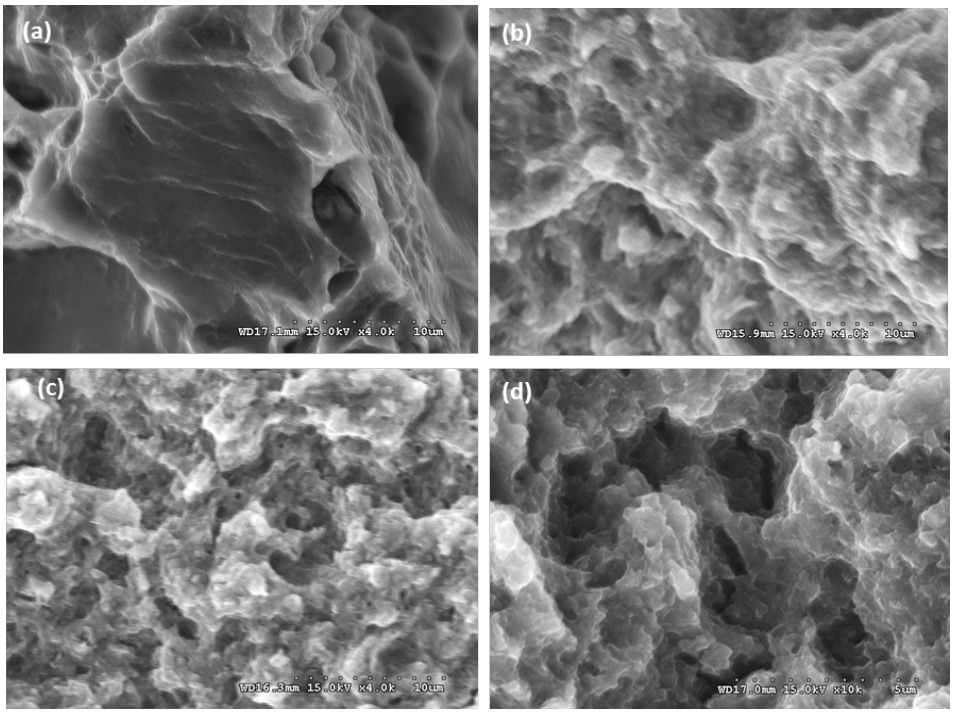

Fig. 4. Fracture surfaces of the deformed tensile specimens: (a) un-milled sample, (b) 10 hrs milled sample, (c) 20 hrs milled sample and (d) 30 hrs milled sample

Figure 5 depicts the loading rate-dependent micro indentation behavior of microcrystalline and nanocrystalline Mg-3%Al alloy samples. The relationship between indentation load (P) and penetration depth (h) of the loading curve was described by Kick's law, and is typically represented by a parabolic relationship, $P = Ch^2$. Here, C is a constant that depends on the shape of the indenter point and the properties of the tested material. Later, Andrews et al. [12] suggested that the value of C would be a function of loading speed as well. In reality, the P–h curve would have the form $P = Ch^{\alpha}$, and the exponent, α is not equal to 2. Thus, it is obvious that both loading rate and microstructure considerably affect the mechanical response of indented material. It is evident for all samples that slower loading speed results in a greater residual indentation depth at the maximum load of 5000 mN. The curvature of the loading segment corresponds to the exponent (α) value. For microcrystalline samples, the loading rates at the segment below ~ 2500 mN of the indentation load behave oppositely to those of the upper segment. In contrast, the curvature of the loading segments increases with increasing loading rates in nanocrystalline samples fabricated from milled powder (except for the 30 h milled sample with 1000 mN/min loading rate). These findings demonstrate that the localised contact on the micostructure is a highly rate-dependent process, and the material response could be described by variations in dislocation density beneath the indenter. For each test, the creep displacement slightly varied at the maximum force hold duration. Dislocation motion was most likely responsible to produced this creep. Based on the load-displacement data obtained from the loading and unloading curves, the elasto-plastic properties of the indented materials were measured in the form of micro-hardness and elastic modulus.

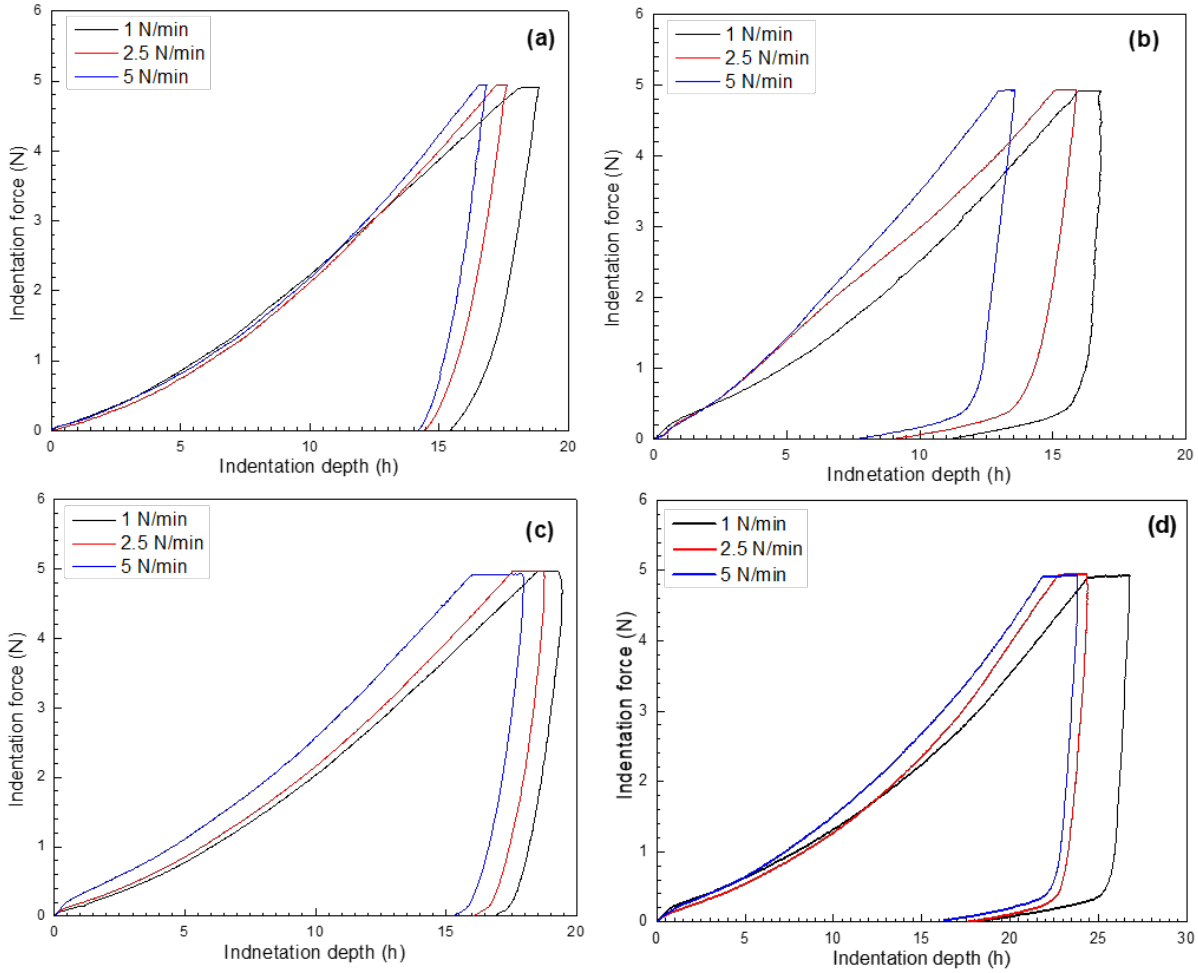

Fig. 5. Loading rate dependent indentation curves for (a) unmilled extruded sample, (b) 10 h milled sampled, (c) 20 h milled sample, and (d) 30 h milled sample.

The indentation depth, microhardness, and indentation modulus of each batch of alloy samples under three different loading rates are presented in Table 2. The indentation force vs depth curve was used to estimate the traditional micro hardness (Vickers) while taking into account the following relationship:

$$H_v = \frac{1.854P}{d^2} \qquad \text{with} \qquad d = 7.006 \times h \qquad (1)$$

where parameter P is the indentation force in N, d is the mean diagonal length in mm, h is the indentation depth in mm, and Hv is the Vickers hardness in N/mm^2 or MPa. Herein, the materials are extremely sensitive to the rate of deformation, and as time and elastic recovery were influencing variables, the mechanical properties of the materials changed dramatically. The results revealed the decrease in loading rate led to an increase in indentation depth, resulting a reduction in the hardness values for each batch of the samples. The variations in geometrically necessary dislocations (GNDs) can directly affect the hardness values [13-14]. The strain gradient theory suggests that a lower density of statically stored dislocations (SSDs) contributes to a higher hardness value at a lower indentation depth. On the other hand, the sample obtained from 10 h milled powder can be shown to have the highest hardness value for all loading rates. The grain refinement, introduction of lattice strain, and Al solid solution hardening may be possible causes of the increase in hardness. It is worth noting that the hardness values decreased in samples prepared after 10 h of milled powder, despite the usual tendency that the hardness value improves with increasing milling duration according to the Hall-Petch relationship between strength and grain size. This discrepancy may be described by the disintegration of Mg-Al solid solution in accordance with changes in Mg lattice parameter and lattice strain recovery. During longer milling times, the supersaturated Mg/Al solid solution seemed to decompose, resulting in a softening of the alloy.

Loading rate →	**5 N/min**			**2.5 N/min**			**1 N/min**		
Milling Time (hrs.) ↓	$h_{pen.}$ (μm)	Hv (MPa)	$E_{ind.}$ (GPa)	$h_{pen.}$ (μm)	Hv (MPa)	$E_{ind.}$ (GPa)	$h_{pen.}$ (μm)	Hv (MPa)	$E_{ind.}$ (GPa)
0	16.8	670.3	27.9	17.67	605.9	33.5	18.8	535.2	28.9
10	13.5	1038.0	51	15.5	787.4	36.5	16.8	670.2	27.8
20	18.0	583.8	37.2	18.7	541.0	37.7	20.1	468.2	45.4
30	23.8	333.9	47.5	24.4	317.7	39.0	25.4	293.2	51.6

*h_{pen} → penetration depth, H_v → Hardness value, and E_{ind}→ indentation modulus.

Table 2. Room temperature tensile properties of Mg/3%Al alloy at different strain rates

The results of elastic modulus exposed that the elasto-plastic behaviors of the extruded samples were not evenly altered with the loading rate of the indentations and the samples derived from different milling durations. There might be several causes behind the dispersed elastic modulus readings. The material deforms both elastically and plastically during the indentation. During unloading of indentation, the materials exhibited a combination of elastic recovery and reverse plasticity. Due to the fact that the first unloading might not be completely elastic, and the calculation of the elastic modulus from the first unloading curves can occasionally give inaccurate results. The extra reverse plasticity raised the elastic modulus by enhancing the slope of the unload curve. Internal stresses in a loaded material become "unstable" during unloading, which may result in reverse plasticity. Last but not least, during unloading, the pinned dislocations relax, the grain boundary adjust, and even phase transition can also affect the elastic modulus.

4. CONCLUSIONS

In conclusion, the extruded Mg–3%Al alloys studied in this work were successfully fabricated from the consolidated mechanically alloyed powders using powder metallurgy route. High yield strength as well as reasonable ductility were achieved within the first 10 hrs of milling as a result of potential strengthening mechanisms like solid solution strengthening and grain refining, as well as particle dispersion strengthening. In contrast, higher milling duration leads Mg(Al) solid solution to become softer. Low yield strength was noted in the samples that received from 20 hrs and 30 hrs of milling, and the earlier strengthening mechanisms seemed to lose their effectiveness throughout the plastic deformation. Enhanced ductility without any appreciable work hardening behaviour can be seen in both 20 hrs and 30 hrs of milled samples. The alloys obtained from the different milling durations displayed strain rate sensitivity. The strain rate dependent deformation behaviours during tensile tests at room temperature, indicating that the values of tensile strengths are increased at higher strain rates.

ACKNOWLEDGMENTS

The corresponding author wishes to express gratitude to the Department of Mechanical Engineering, NUS, Singapore, for providing the resources for the development of the Mg-3% Al alloys.

REFERENCES

1. Song, J, She, J, Chen, D, Pan, F 2020, “Latest research advances on magnesium and magnesium alloys worldwide”, *Journal of Magnesium and Alloys*, vol. 8, no. 1, pp. 1–41.
2. Gupta, M 2020, “Magnesium: The Wonder Element for Engineering/Biomedical Applications”, *Intechopen*, London, UK.
3. Xu, T, Yang, Y, Peng, X, Song, J, Pan, F 2019, “Overview of advancement and development trend on magnesium alloy”, *Journal of Magnesium and Alloys*, vol. 7, no. 3, pp. 536-544.
4. Liu, H, Huang, H, Yang, X, Li, C, Yan, J, Jiang, J, Ma, A 2017, “Microstructure and mechanical property of a high-strength Mg–10Gd–6Y–1.5 Zn–0.5 Zr alloy prepared by multi-pass equal channel angular pressing”, *Journal of Magnesium and Alloys*, vol. 5, no. 2, pp. 231-237.
5. Kujur, MS, Manakari, V, Parande, G, Prasadh, S, Wong, R, Mallick, A, Gupta, M 2021, “Development of rare-earth oxide reinforced magnesium nanocomposites for orthopaedic applications: A mechanical/immersion/biocompatibility perspective”, *Journal of the Mechanical Behaviour of Biomedical Materials*, vol. 114, pp. 104162.
6. Chua, BW, Lu, L, Lai, MO 2006, “Deformation behaviour of ultrafine and nanosize-grained Mg alloy synthesized via mechanical alloying”, *Philosophical Magazine*, vol. 86, no. 19, pp. 2919-2939.
7. Mallick, A, Vedantam, S, Lu, L 2009, “Grain size dependent tensile behavior of Mg–3% Al alloy at elevated temperatures”, *Materials Science and Engineering: A*, vol. 515, no. 1-2, pp. 14-18.
8. Agnew, SR, Duygulu, Ö 2005, “Plastic anisotropy and the role of non-basal slip in magnesium alloy AZ31B”, *International Journal of plasticity*, vol. 21, no. 6, pp. 1161-1193.
9. Wang, H, Raeisinia, B, Wu, PD, Agnew, SR, Tomé, CN 2010, “Evaluation of self-consistent polycrystal plasticity models for magnesium alloy AZ31B sheet”, *International Journal of Solids and Structures*, vol. 47, no. 21, pp. 2905-2917.
10. Zhang, X, Wang, Z, Jiang, Y, Sun, G, Jiang, Z, Che, C, Fang, D 2018, “Strain Rate Dependence of Tensile Properties of Extruded Mg–9Y–3Zn–1Mn Alloy”, *Advanced Engineering Materials*, vol. 20, no. 9, pp. 1800123.

11. Sabirov, I, Barnett, MR, Estrin, Y, Hodgson, PD 2009, "The effect of strain rate on the deformation mechanisms and the strain rate sensitivity of an ultra-fine-grained Al alloy", *Scripta Materialia*, vol. 61, no. 2, pp. 181-184.
12. Andrews, EW, Giannakopoulos, AE, Plisson, E, Suresh, S 2002, "Analysis of the impact of a sharp indenter", *International journal of solids and structures*, vol. 39, no. 2, pp. 281-295.
13. Pharr, GM, Herbert, EG, Gao, Y 2010, "The indentation size effect: a critical examination of experimental observations and mechanistic interpretations", *Annual Review of Materials Research*, vol. 40, pp. 271-292.
14. Nix, WD, Gao, H 1998, "Indentation size effects in crystalline materials: a law for strain gradient plasticity", *Journal of the Mechanics and Physics of Solids*, vol. 46, no. 3, pp. 411-425.